Available online at www.sciencedirect.com
ScienceDirect
Journal of Catalysis 256 (2008) 45–61
JOURNAL OF CATALYSIS
www.elsevier.com/locate/jcat

V_2O_5–SiO_2 systems prepared by flame pyrolysis as catalysts for the oxidative dehydrogenation of propane

I. Rossetti [a], L. Fabbrini [a], N. Ballarini [b], C. Oliva [a], F. Cavani [b], A. Cericola [b], B. Bonelli [c], M. Piumetti [c], E. Garrone [c], H. Dyrbeck [d], E.A. Blekkan [d], L. Forni [a,*]

[a] *Dipartimento CFE e ISTM-CNR, Università di Milano, via C.Golgi, 19 20133 Milano, Italy*
[b] *Dipartimento di Chimica Industriale e dei Materiali, Università di Bologna, INSTM, Research Unit of Bologna, NoE Idecat partner (FP6 of EU), Italy*
[c] *Dipartimento di Scienza dei Materiali ed Ingegneria Chimica, Politecnico di Torino, Torino, INSTM Unit Torino Politecnico, Italy*
[d] *Department of Chemical Engineering, Norwegian University of Science and Technology, N-7491 Trondheim, Norway*

Received 13 December 2007; revised 25 February 2008; accepted 27 February 2008

Available online 2 April 2008

Abstract

VO_x/SiO_2 catalysts were prepared through an innovative flame pyrolysis (FP) technique and tested for the oxidative dehydrogenation of propane. The samples, of different V loadings, were characterized by electron paramagnetic resonance (EPR), micro-Raman, and FT-IR spectroscopy to assess the nature of the vanadium active sites in comparison with a sample prepared by impregnation. The active sites of the FP-prepared catalysts appeared as highly dispersed $V^{5+}O$ groups partly incorporated into the silica matrix and interacting poorly with one another. Lower dispersion can be achieved at the same V loading with the catalyst prepared by impregnation. EPR revealed $V^{4+}O$ groups pointing out normally from the catalyst surface and sitting in the center of a surface array of oxygen atoms. These V^{4+} groups helped demonstrate the difference in catalytic behavior of the various samples. Catalytic activity measured under both aerobic and anaerobic conditions revealed a promisingly high selectivity with the FP-prepared samples. The best results were obtained with a 10 wt% V loading, which provided the best propylene yield among the samples, especially under anaerobic conditions (up to 80% selectivity at 10% propane conversion). This is likely related to the much higher dispersion of the VO_x species in the FP-prepared samples, which also helps reduce the coke formation triggered by exposed surface acid sites.

Keywords: Propane ODH; Flame pyrolysis; Silica-supported vanadium; Anaerobic and co-feed reaction conditions

1. Introduction

Oxidative dehydrogenation (ODH) of light alkanes offers a potentially attractive route to alkenes, because the overall reaction pathway is exothermic, and the thermodynamic constraints of nonoxidative routes are avoided [1–5]. Furthermore, carbon deposition is limited, allowing for more stable catalytic activity. However, the yield of alkenes obtained on most catalysts is decreased by parallel or consecutive reactions, mainly the combustion of reactant and products to CO and CO_2 and formation of oxygenated byproducts, such as acetic acid [6]. Along with selectivity problems, the co-feeding of oxygen also can entail risks, which can be decreased through appropriate process engineering. On the other hand, selectivity problems also can be partly overcome by optimizing the catalyst formulation.

Among the possible active phases, V oxide (VO_x) has been the most widely investigated, because when loaded in a proper amount on a suitable support, it leads to promising yields of ethylene [7–10], propylene [6,7,11,12], or butenes [8]. Many different supports have been tested, including ZrO_2 [13,14], TiO_2 [12], V-substituted zeolites or silicalites [15], SiO_2 [9,13,16], and Al_2O_3, usually as the γ-phase [6–8,10–13,17]. Most of the previous investigations have examined the effect of V loading in determining active species distribution and the role of the support on V surface dispersion. The acidity of the support can negatively affect selectivity when low V loading leaves

* Corresponding author. Fax: +39 02 50314300.
E-mail address: lucio.forni@unimi.it (L. Forni).

0021-9517/$ – see front matter
doi:10.1016/j.jcat.2008.02.028

naked acid sites, particularly in the case of alumina-supported samples [8].

The reaction can be kinetically modeled through a Mars–van Krevelen mechanism centered on V reduction and subsequent reoxidation [6,12]. Indeed, the first reaction step involves V^{5+}, which reduces to V^{4+} and then to V^{3+}. The active oxidized VO_x sites can be promptly restored by oxygen when co-fed with the paraffin. The nature of such active sites has been widely investigated [13,18,19]; it seems that V^{5+} is dispersed on the support in the form of isolated vanadate species, which progressively oligomerize and polymerize with increasing V loading until a monolayer is formed. Different V loadings and/or V surface densities corresponding to monolayer formation have been reported, depending on the support and on calcination conditions [10,13,18,20,21]. High activity is ascribed to vanadate species, either isolated or polymerized up to the formation of a VO_x monolayer, whereas lower activity is usually associated with the presence of bulk V_2O_5. As for selectivity, a possible role of the support cannot be excluded, especially with samples characterized by strong Lewis acidity [11]. In such cases, high selectivity can be achieved when a VO_x monolayer completely covers the support. V loading corresponding to monolayer formation is different for different supports, depending on the V–support affinity. It has been shown [13] that samples supported on SiO_2 mainly constitute isolated VO_x species up to a surface density of ca. 2 V/nm^2. On a further increase in V loading, V_2O_5 formed, thereby diminishing catalyst performance. In contrast, alumina- or titania-supported samples showed higher surface density (7–8 V/nm^2), corresponding to polymeric vanadyl species. With the latter supports, it was difficult to attain high V dispersion except by excessively decreasing V loading, with a consequent deterioration of catalytic activity.

The catalysts described so far are usually prepared by impregnation, leading to deposition of vanadium onto the surface of the selected support. To the best of our knowledge, to date no study has been carried out on the possible preparation of nanostructured V-supported catalysts for the present application. A new procedure based on flame pyrolysis (FP) of an organic solution of metal ion precursors has been devised for the preparation of different single or mixed oxides [22–29]. Consequently, the catalysts considered in the present work were prepared by FP, with the aim of developing systems in which the active component is dispersed inside the inert matrix (silica in the present case) instead of being deposited over it. In principle, the dilution inside porous silica should allow better dispersion of the active component, thereby providing also better control of the heat generated by the reaction and hence a decrease in local hot spots, which may be detrimental to process selectivity. A similar result can be achieved by the sol–gel method, which also leads to the incorporation/occlusion of metal oxide nanoparticles inside silica [30] or alumina. But with respect to the sol–gel method, FP offers the advantage of (i) better control of the preparation procedure and hence of the physicochemical properties of the final material, and (ii) preferred formation of nanosized agglomerates. Furthermore, the classical preparation procedures for silica- (or siliceous materials-) supported vanadium oxide catalysts make use of high-surface area supports [16,30]. Generally, silica supports have a microporous structure, making them unsuitable for selective oxidation reactions. In contrast, the FP method usually leads to poorly porous materials with surface areas not exceeding 150 m^2/g [22–29]. This may represent another advantage of this preparation procedure over conventional techniques.

Table 1
Composition and SSA of the prepared catalysts. Values in parentheses represent SSA due to micropores contribution as determined by t-plot

Sample	$V_2O_5/(V_2O_5 + SiO_2)$ (wt%)	SSA (m^2/g)
SiO_2	–	14 (6)
V5Si	5.0	41 (14)
V10Si	10.0	75 (n.d.)
V28Si	28.4	80 (n.d.)
V50Si	50.0	46 (8.6)
V10Si-i[a]	10.0	–

[a] Prepared by impregnation of the FP-prepared support.

The aim of the present work was to prepare by FP a set of nanostructured V-based catalysts characterized by different V loadings and to compare their performance in the ODH of propane with that of a sample prepared by impregnating a FP-prepared silica by a traditional procedure. All of the samples were characterized by several physicochemical techniques, and their activity was tested under different reaction conditions, under a co-feed of propane and oxygen and under anaerobic conditions (i.e., simulating an alternate feed of propane and air) [17,31–34].

2. Experimental

2.1. Catalyst preparation

A detailed description of the FP preparation procedure and of the effect of the main operating parameters on catalyst properties can be found elsewhere [23–26]. In brief, proper amounts of vanadium(IV) oxy-acetylacetonate (Merck, 98%) and tetraethyl-orthosilicate (TEOS, Aldrich 99,999%), were dissolved in an organic solvent (alcohol, carboxylic acid, or a mixture of the two) to obtain a 0.1–0.2 M solution (concentration referring to the nominal oxide composition). The solution was fed at a rate of 4.4 cm^3/min to the FP burner, together with 5.0 L/min of oxygen (SIAD, purity >99.95%). The cross-sectional area of the burner nozzle was adjusted so as to maintain a pressure drop of 0.4 bar along it. The main flame was ignited and supported by a ring of 12 premixed $O_2 + CH_4$ flamelets (CH_4 = 0.5 L/min; O_2 = 1.0 L/min). The catalyst powder so produced was collected by means of a 10-kV electrostatic precipitator [23,35]. The yield was 90–95% for each sample, the compositions of which are reported in Table 1. The comparative catalyst (V10Si-i in Table 1) was created through impregnation of a FP-prepared SiO_2 batch with NH_4VO_3 solution, followed by drying and calcination at 700 °C in air.

2.2. Catalyst characterization

Specific surface area (SSA) was measured by N_2 adsorption/desorption at the temperature of liquid nitrogen on a Micromeritics ASAP 2010 apparatus. Microporosity, when relevant, was determined by the *t*-plot procedure. Morphological analysis was done with a LEICA LEO 1430 scanning electron microscope. XRD analysis was conducted using a Philips PW1820 powder diffractometer with a Ni-filtered Cu$K\alpha$ radiation source ($\lambda = 1.5148$ Å). The diffractograms thus obtained were compared with literature data for phase recognition [36]. Thermogravimetric analysis (TGA) of the as-prepared powder was done in flowing air using a Perkin–Elmer TGA7 analyzer. Electron paramagnetic resonance (EPR) spectra were collected between −153 and 27 °C in air using a Bruker Elexsys instrument, equipped with a standard rectangular ER4102ST cavity and operated at X band, 6.36-mW microwave power, and 100-kHz Gauss modulating amplitude. The intensity of the magnetic field was carefully checked with a Bruker ER35M Teslameter, and the microwave frequency was measured with a HP 5340A frequency meter. Spectral simulations, when required, were done using the Bruker SimFonia program.

Laser-Raman spectra were obtained using a Renishaw 1000 instrument coupled with a Linkam thermal cell TS 1500; the samples were excited with the 514-nm Ar line under N_2 atmosphere. For FT-IR measurements in the low wavenumber range, powder samples were mixed with optical-grade KBr. For further FT-IR measurements, powder samples were pressed into thin, self-supporting wafers and pretreated in high vacuum (residual pressure $<10^{-3}$ mbar) using a standard vacuum frame, in a IR cell equipped with KBr windows. Spectra were collected at 2-cm^{-1} resolution on a Bruker FTIR Equinox 55 spectrophotometer equipped with an MCT detector. To remove moisture and other atmospheric contaminants, the wafers were outgassed for 1 h at 150, 300, and 500 °C before adsorption of CO or NH_3. CO adsorption spectra were collected at the temperature of liquid nitrogen by dosing increasing amounts of CO (in the 0.05–15.0 mbar equilibrium pressure range) on outgassed samples, inside a special quartz IR cell that allowed simultaneous dosing of carbon monoxide and addition of liquid N_2. NH_3 was dosed at room temperature in the 0.01–23.0 mbar equilibrium pressure range, after which the reversible fraction of adsorbate was removed by prolonged evacuation. After each experiment, an evacuation step was performed to study the reversibility of the interaction.

2.3. Catalytic activity tests

Catalytic activity was measured by means of a continuous quartz tubular reactor (7 mm i.d.) heated by an electric furnace. The catalyst (0.90 mL, 0.5–0.6 g, 425–600 μm particle size) was activated before each run in 20 cm^3/min of flowing air as the temperature was increasing by 10 °C/min up to 550 °C, then maintained there for 1 h. The flow rate of the reactant mixture for the co-feeding mode test was 11 cm^3/min of C_3H_8 (20 mol%) + 11 cm^3/min of O_2 (20 mol%) + 28 cm^3/min of He + 4 cm^3/min of N_2 (60 mol% inert). For the anaerobic mode, flow rates were 6 cm^3/min of C_3H_8 (22 mol%) + 19 cm^3/min of He + 2 cm^3/min of N_2. Contact time was 1 s for the former testing mode and 2 s for the latter testing mode. The exiting gas was analyzed by means of a micro gas chromatograph (Agilent 3000A), equipped with Plot-Q, OV-1, and MS-5A columns for complete detection of the effluent products. Propane conversion was calculated as the conversion over fed propane mol. The selectivity to the *i*th product was calculated as mol of generated *i*th species over mol of converted propane, normalized with respect to the reaction stoichiometry. Carbon balance was calculated as the sum of selectivity to the various species.

3. Results and discussion

3.1. Catalyst preparation and characterization

Solubility tests revealed that the best solvent with fuel properties for the V precursor was ethanol, whereas good miscibility of the Si precursor was found with both ethanol and propionic acid. But when the latter solvent was used in a 1:1 (vol/vol) ratio with the ethanol solution of V, some problems were encountered at low V loadings (⩽10%), involving a much more difficult precursor decomposition in the flame. This very likely was due to the lower amount of VO_x phase formed, which plays a role in catalyzing the oxidation of both the solvent and the organic compounds during synthesis (*vide infra*). Furthermore, a lower flame temperature was attained with the ethanol + propionic acid mixture, likely leading to greater surface area and smaller particle size with respect to the ethanol + 1-octanol fuel mixture [26], which was added to increase the combustion enthalpy of the solvent mixture.

During FP, complete combustion of the organic compounds (both solvent and reagents) should be achieved, along with simultaneous formation of the desired oxides. However, some unburnt carbonaceous residue usually is found in the latter; their amounts can be estimated through TGA analysis in flowing air (Table 2). Basically, two peaks were observed, one at low temperature (80–170 °C), attributed to residual solvent, and the other at higher temperature (500–550 °C), attributed to unburnt carbonaceous species. At low V content, the area of the lower-temperature TGA peak was comparable to that of the high-temperature TGA peak. Furthermore, the latter shifted toward lower temperature and decreased in intensity with increasing V-loading. This indicates that during catalyst preparation, the presence of a phase active for oxidation reactions facilitates precursor decomposition. In addition, the samples with

Table 2
Weight loss during TGA analysis and temperature of the main peaks observed

Sample	1st peak *T* (°C)	2nd peak *T* (°C)	Total wt% loss	2nd peak wt% loss
SiO_2	80	515	3.7	1.7
V5Si	170	550	6.3	1.4
V10Si	170	520	2.9	0.7
V28Si	90	520	7.8	1.0
V50Si	105	495	5.5	0.3

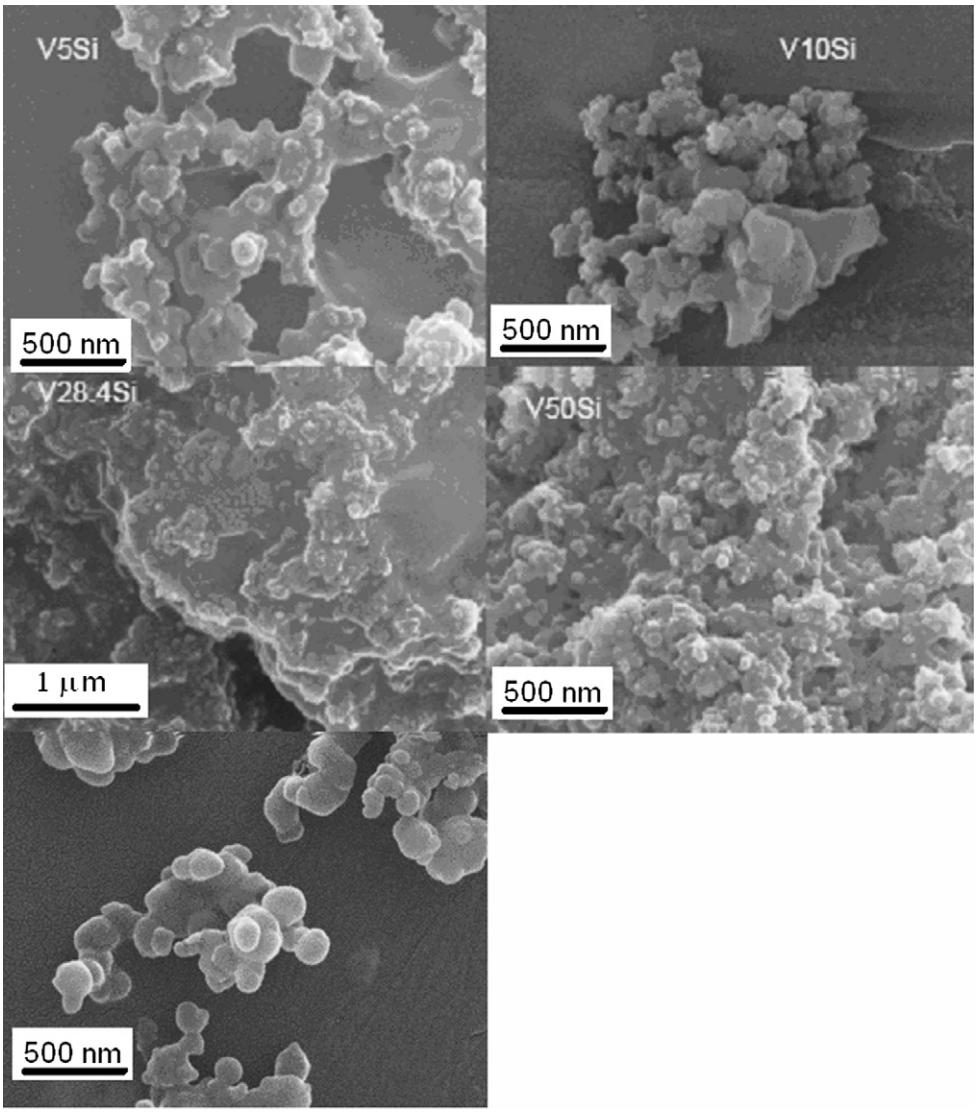

Fig. 1. SEM micrographs of the prepared samples. Marker size: 500 nm except for V28Si (1 μm).

low V-loading also demonstrated additional peaks between 150 and 350 °C, confirming the difficult decomposition of the precursors.

XRD analysis revealed amorphous or sub-microcrystalline powders only, along with the absence of V-based phases for V loadings <28%. A fully reliable V-based phase identification was possible only for the V50Si sample, which demonstrated the V_2O_5 phase reflection peaks [36, file 009-0387]; however, these results must be compared with those from Raman and IR spectroscopy (*vide infra*), which can reveal the presence of vanadia down to V loadings below than that demonstrated by XRD.

SEM images (Fig. 1) showed a poorly defined morphology for every sample, likely associated with the amorphous structure. However, at high V loading (V50Si), the sample seemed to organize in small (ca. 100 nm) spheroidal particles.

Our findings are partly associated with the nature of the selected materials and partly associated with solvent/fuel choice. Indeed, the use of alcohols did not yield small and homogeneous particle sizes for other catalyst compositions [27,28]; however, the increased particle size uniformity at high V loadings seems to confirm the beneficial effect of this element during catalyst preparation.

SSA was minimal for the pure silica support (Table 1), increased with increasing V loading up to 28% V (sample V28Si), and then decreased thereafter. Higher SSAs can be expected when using carboxylic acids, basically because of their decomposition route, involving acid decarboxylation with formation of a low-boiling alkane, allowing further fragmentation of the forming particles during solvent flash [37]. Comparing microporous area (as determined by *t*-plot analysis) with BET SSA (Table 1) demonstrates that despite the low surface area of SiO_2, 44% of that value can be ascribed to the contribution of micropores. It should be noted that in the FP-prepared nanosized samples, microporosity is likely related to interparticle voids rather than to intraparticle porosity. On the addition of V, micropore surface area decreased progressively with increasing V loading. Keeping in mind the aforementioned considerations on catalyst

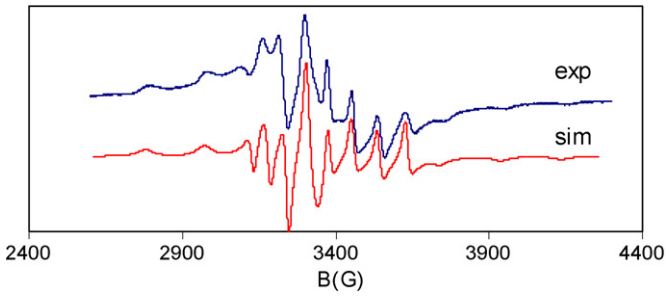

Fig. 2. EPR spectrum of sample V50Si. Upper track, experimental; lower track, computer simulation with the spectral parameters reported in Table 3 and corresponding to isolated (monovadates) $V^{4+}O_x$ species.

Table 3
EPR experimental parameters

	$g_\parallel$	$g_\perp$	B[a]	$A_\parallel$ (G)	$A_\perp$ (G)	$\Delta W_\parallel$ (G)[b]	$\Delta W_\perp$ (G)[b]
V10Si	1.940	1.985	3.60	194	77	20	15
V10Si-i	1.942	1.985	3.50	194	77	20	15

[a] From Eq. (1).
[b] Lorentzian-shaped line width.

morphology, the decrease in particle size can be indirectly confirmed. Indeed, a slightly higher surface area was obtained with increasing V loading (along with a decreased contribution of micropores).

3.2. EPR analysis

The EPR spectral profile of the VO_x/SiO_2 samples was nearly independent of V loading, whereas the samples' spectral intensity increased ca. fourfold with increasing V concentration from 5 to 10%, then remained approximately constant at higher V concentrations. Fig. 2 compares the most intense EPR pattern, obtained with the V50Si sample, with the simulation obtained with the parameters reported in Table 3, which are typical of V^{4+} ions.

With V_2O_5/SiO_2 catalysts, EPR spectra of this kind have been attributed to V^{4+} species in monolayers and double layers of V_2O_5 supported on SiO_2 in average C_{4v} symmetry [38,39]. This corresponds to an array of oxygen ligands lying parallel to the surface around a V^{4+}–O bond perpendicular to it. The finding that $g_\parallel < g_\perp$ can be attributed to tetragonal distortion. It has been shown [40] that a higher value of the parameter

$$B = (g_\parallel - g_e)/(g_\perp - g_e) \quad (1)$$

indicates a shortened V^{4+}–O bond or an increased distance of the oxygen ligands in the basal plane. Both of these situations would lead to strengthening of the V^{4+}–O bond. In the present case, $B \cong 3.60$ (Table 3) is considerably higher than the values obtainable with the data reported previously for SiO_2–V^{4+} monolayers (B ca. 2.41–3.10) and SiO_2–V^{4+} double layers (B ca. 2.24–2.65) [40]. Thus, our relatively high value for B indicates that no more than a monolayer of SiO_2–V^{4+} was present on the surface.

Thermal treatment *in vacuo* at 300 °C, with likely consequent loss of oxygen, had no significant effect on the spectral

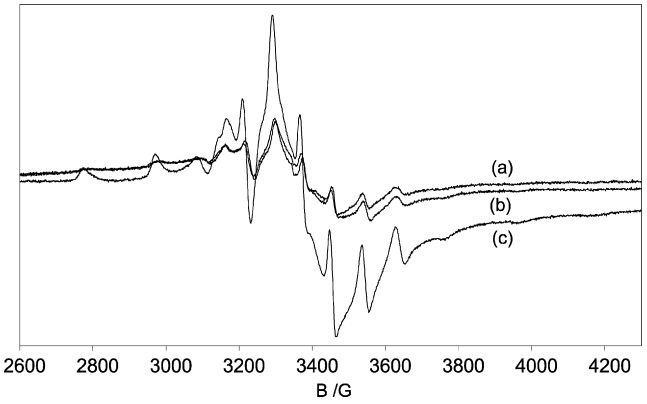

Fig. 3. EPR spectra at r.t. of sample V28Si: (a) as prepared, (b) after deoxygenation, (c) after catalytic use under anaerobic conditions and deoxygenation.

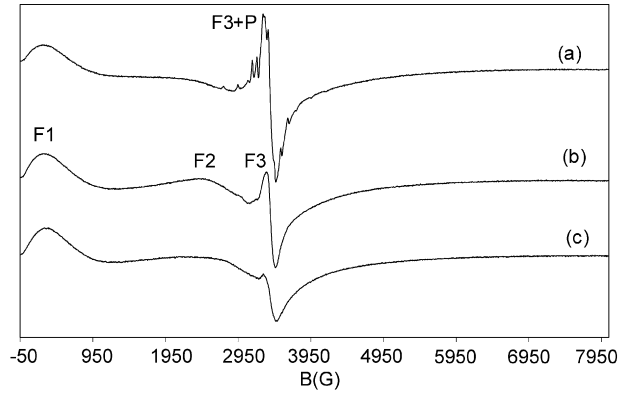

Fig. 4. EPR spectra of sample V10Si-i at (a) −154 °C, (b) 25 °C and (c) 127 °C. F1, F2 and F3 indicate ferromagnetic resonance features.

profile and sometimes simply increased its intensity slightly (Fig. 3b). In contrast, the spectral intensity increased markedly after the catalytic reaction under anaerobic conditions (Fig. 3c); this can be explained by considering that the catalytically active centers are V^{5+}, which reduce during reaction in the absence of co-fed oxygen, leading to an increase in the EPR-active V^{4+} species. Therefore, the latter represent an intermediate of the catalytic process.

Unlike FP samples, which exhibited EPR spectra related to isolated V^{4+} species, the spectrum of the V10Si-i sample comprised three regions (Fig. 4): the first (F1) centered at ca. 250 G, the second (F2) centered at ca. 2500 G, and the third (F3) centered at ca. 3390 G (corresponding to $g = 1.98$). Bands like these have been attributed to ferromagnetic resonance (FMR) of clusters of particles of different shapes and sizes [41–45]. Systems of this kind were not observed with our FP-prepared samples, in which the V-based active centers were likely dispersed uniformly and not interacting with each other.

A further paramagnetic contribution, P, was added to F3 (Fig. 4a). Its hyperfine pattern can be easily interpreted by subtracting the component F3 of the spectra of Fig. 4 spectrum b or c (multiplied by a proper factor) from the spectral region F3 + P of spectrum a. In this way, the EPR pattern P appeared, very similar to that of the FP samples (Fig. 2). The only difference is that here the value of $g_\parallel$, 1.942, is slightly higher

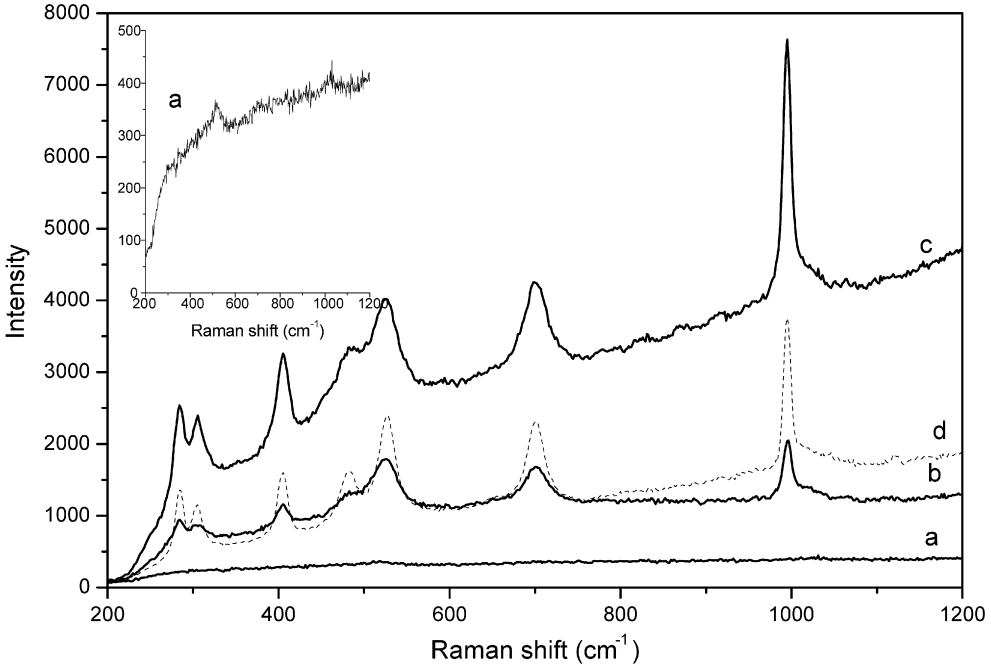

Fig. 5. Raman spectra, in the 200–1200 cm^{-1} range, recorded with samples V10Si, V28Si, V50Si and V10Si-i (curves a, b, c and d, respectively). Inset to figure: magnification of curve a (V10Si).

than that of 1.940 characterizing the FP-prepared sample. The spectral simulation (not reported) confirms this very small difference, leading to a value $B \cong 3.5$ for V10Si-i, lower than the value $B = 3.6$ found for V10Si, the former corresponding to a slightly lower V^{4+}–O bond strength in the V10Si-i catalyst.

3.3. Micro-Raman spectroscopy

Fig. 5 reports the Raman spectra of powder samples in the 200–1200 cm^{-1} range. The inset reports the magnified spectrum of sample V10Si (curve a), which shows two weak bands at 1027 and 512 cm^{-1}, which can be readily assigned to isolated V=O species [46]. At higher V loadings (curves b and c) and with sample V10Si-i (dotted curve d), the typical bands of crystalline V_2O_5 can be seen at 285, 304, 404, 482, 525, 701, and 995 cm^{-1} [46–48], whereas no bands were observed on the V5Si sample, which had the lowest V content (results not reported). On the whole, monovanadates were detected only with sample V10Si, whereas both at higher V loadings and after impregnation, the preferential formation of bulk vanadia occurred.

Possibly formed even with silica-supported samples prepared following this new synthetic procedure, oligomeric species would be evidenced by the appearance of Raman bands at 750–900 cm^{-1} due to V–O–V stretching in spectra collected on dehydrated samples. In contrast, the band appearing at 1027 cm^{-1} in dehydrated samples and ascribed to V=O is due to both isolated and oligomeric species. Raman spectra of the V10Si sample are reported in Fig. 6, with the data collected with prolonged accumulation to increase the signal resolution. Very intense bands due to monomeric species were present, and no oligomeric species were observed on both the fresh sample and after dehydration at 200 °C. It is interesting that no dramatic change in spectral profile occurred after dehydration.

3.4. FT-IR analysis: KBr pellets

Fig. 7 reports the FT-IR spectra of powders in KBr pellets in the 1500–600 cm^{-1} range, where vibrational modes of the solid absorb. Band envelopes 1 (1300–1100 cm^{-1}) and 2 (ca. 800 cm^{-1}) can be assigned to the asymmetric and symmetric stretch vibrations of Si–O–Si (siloxane) groups of silica, respectively [49]. With all of the samples except V10Si-i (curves a–d), band 3 was seen at 930 cm^{-1}. This band was previously observed in V/silica and V/silicalite systems [48,49] (i.e., amorphous silica and all-silica zeolite incorporating V) and was assigned to the vibration of SiO_4 groups strongly polarized by the presence of framework vanadium. Such species were not seen with the sample obtained by impregnation (dotted curve e), demonstrating the incorporation of vanadium in the silica framework in samples prepared by FP.

At higher vanadium content (curves b–d), a component developed at 1010 cm^{-1} (band 4), which can be assigned [46–48] to crystalline V_2O_5, in agreement with Raman spectra (Fig. 5).

3.5. FT-IR analysis: Hydroxyl spectra

Fig. 8A reports the FT-IR spectra in the hydroxyl range (3800–3100 cm^{-1}) of sample V10Si outgassed at 150, 300, and 500 °C. The spectra exhibited a band at 3745–3742 cm^{-1}, assigned to isolated silanols, which are commonly seen at the surface of amorphous silica [50]. On V10Si outgassed at 150 and 300 °C (curves a and b), the bands of H-bonded silanols appeared as a weak component at about 3720 cm^{-1} (asterisk) and a broad absorption below 3700 cm^{-1}. The former can be assigned to terminal silanols of H-bonded SiOH chains, whereas H-bonded silanols inside the chains absorb below 3700 cm^{-1}

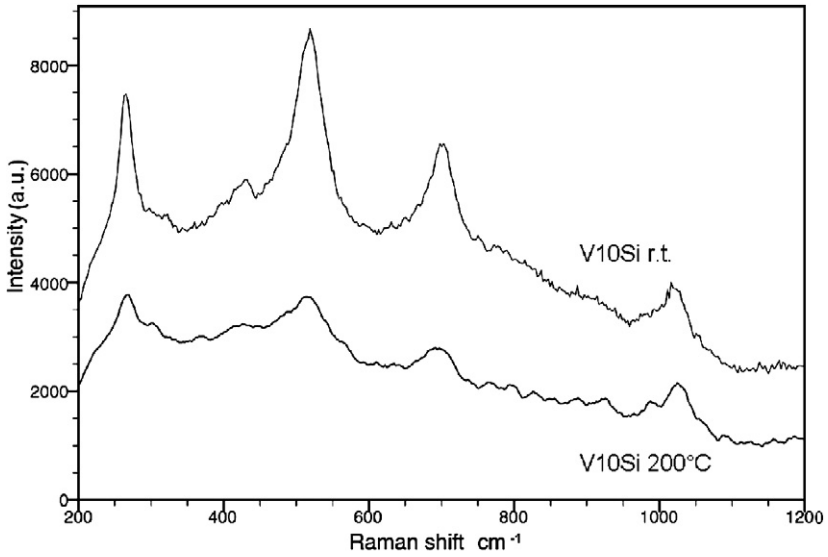

Fig. 6. Raman spectra of sample V10Si (prolonged acquisition time). Comparison between the fresh sample and after dehydration at 200 °C.

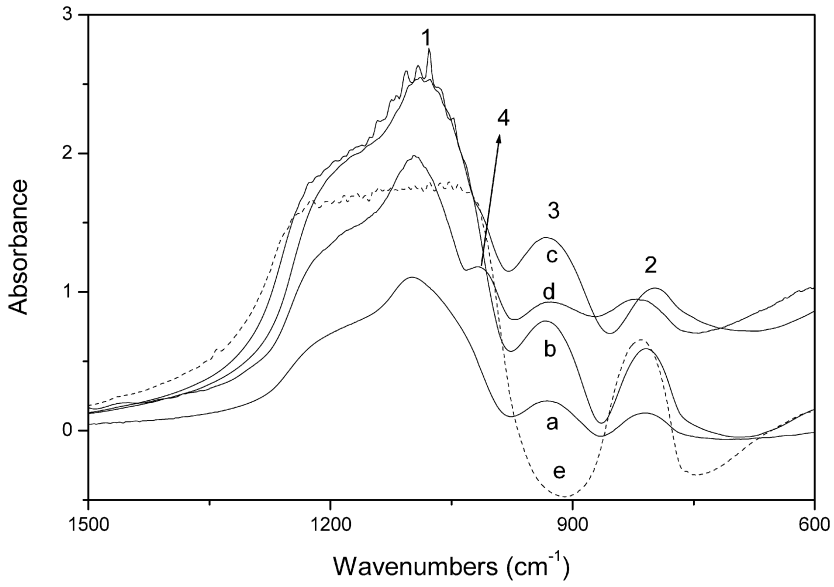

Fig. 7. FT-IR spectra, in the 1500–600 cm^{-1} range of samples V5Si, V10Si, V28Si, V50Si and V10Si-i (curves a, b, c, d and e, respectively) in KBr pellets.

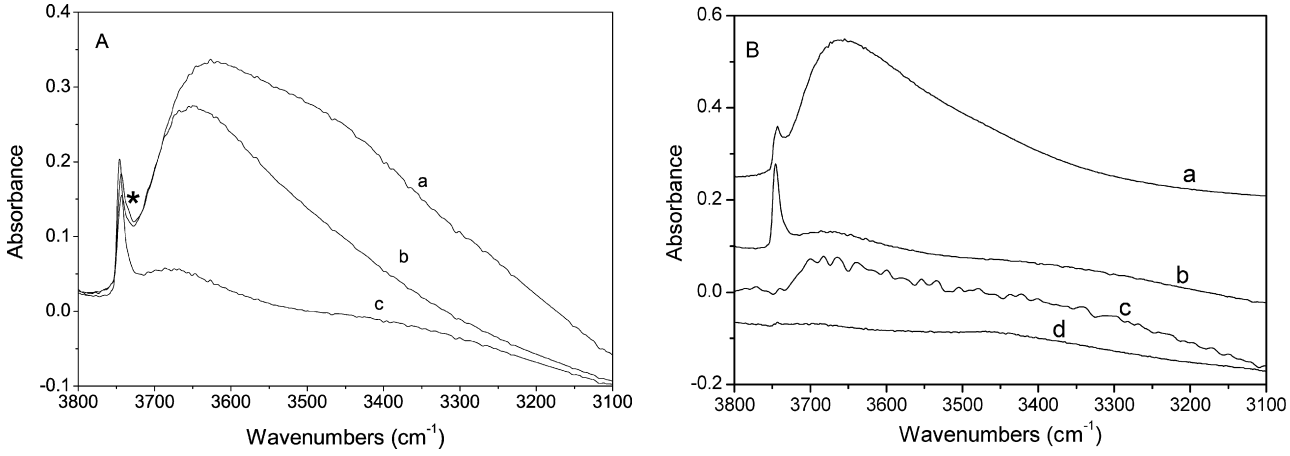

Fig. 8. (A) FT-IR spectra, in the 3800–3000 cm^{-1} range, of sample V10Si outgassed at 150 (curve a), 300 (curve b) and 500 °C (curve c). (B) Normalized FT-IR spectra, in the 3800–3000 cm^{-1} range, of samples V5Si (curve a), V10Si (curve b), V28Si (curve c) and V10Si-i (curve d) out gassed at 500 °C.

[50]. After outgassing at 500 °C (curve c), the band of isolated silanols appeared at 3745 cm^{-1}, along with an ill-defined absorption at about 3680 cm^{-1}, possibly due to defective interparticle silanols [51]. V–OH species, when present, should absorb at about 3675 cm^{-1}; however, due to the abundance of silanols, the corresponding band likely was superimposed on that of H-bonded silanols.

Fig. 8B shows the FT-IR spectra of samples V10Si, V10Si-i, V5Si, and V28Si outgassed at 500 °C. The spectra were normalized to unit specific weight, to compare the hydroxyl populations of the different samples. With V5Si (curve a), bands due to free silanols (3745 cm^{-1}) and H-bonded silanols appeared. With V10Si (curve b), the amount of H-bonded silanols increased, in agreement with its lower vanadium content. At higher vanadium content (V28Si, curve c), no band appeared at 3745 cm^{-1}, and the spectrum became very noisy, in agreement with the sample's decreased transparency, which became dark-green after outgassing at 500 °C. As indicated by Raman spectroscopy data (*vide supra*), the surface of V28Si was covered by V_2O_5, which underwent reduction by annealing under vacuum at high temperature. The ill-observed broad band likely was due to some surface V–OH species. With V10Si-i (curve d), the amount of residual silanols was negligible, likely due to the presence of vanadia, as revealed by the Raman spectra.

3.6. FT-IR analysis: adsorption of NH_3 at rt and of CO at −196 °C

The acidity of surface hydroxyls (isolated and H-bonded silanols, V–OH species) was analyzed by adsorption of basic probes, NH_3 and CO. Fig. 9 shows the difference spectra recorded after dosing NH_3 on sample V10Si, outgassed at 150 and 500 °C, obtained after subtracting the spectra of the bare sample reported in Fig. 8A. After ammonia adsorption on V10Si outgassed at 150 °C, a band grew at 1446 cm^{-1}, assigned to the bending vibration of ammonium species formed on Brønsted hydroxyls. At the same time, bands decreased in the OH stretching region at 3746, 3675, and 3560 cm^{-1}; the first and third of these bands were assigned to free and H-bonded silanols, respectively, interacting with NH_3, whereas the second band was assigned to V–OH species, more acidic than isolated silanols and thus responsible for proton transfer to ammonia (1446 cm^{-1}) [52]. After outgassing at 500 °C, only the band of isolated silanols decreased in the OH stretching range, along with a small component at 3720 cm^{-1}, due to some residual H-bonded silanols (Fig. 9b); after dehydration, the more acidic hydroxyls (V–OH species and H-bonded silanols) were removed. At lower wavenumbers, a band was present at 1606 cm^{-1}, assigned to NH_3 coordinated to vanadium ions performing as Lewis acidic sites, now exposed at the surface. The band of ammonium bending vibration was shifted to higher wavenumbers (1465 cm^{-1}), demonstrating interaction with weaker Brønsted sites (H-bonded silanols absorbing at 3720 cm^{-1}).

Different OH species were detected at the surface of V10Si sample, for which the following scale of acidity may be pro-

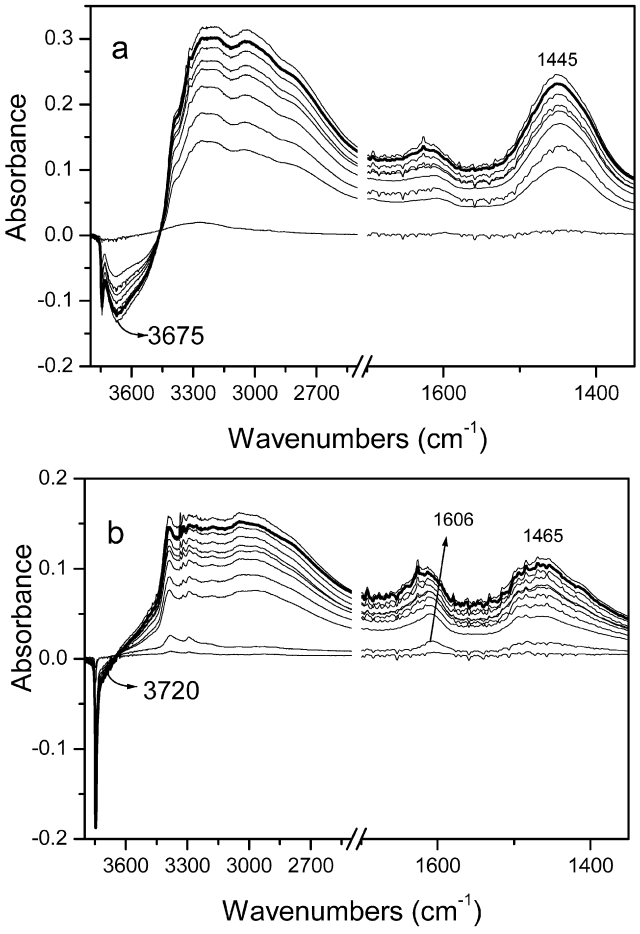

Fig. 9. FT-IR difference spectra recorded after dosing NH_3 at r.t. on sample V10Si out gassed at 150 (a) and 500 °C (b). NH_3 partial pressures in the 0.01–23.0 mbar range. Bold curves: spectra recorded after 30 min out gassing at rt.

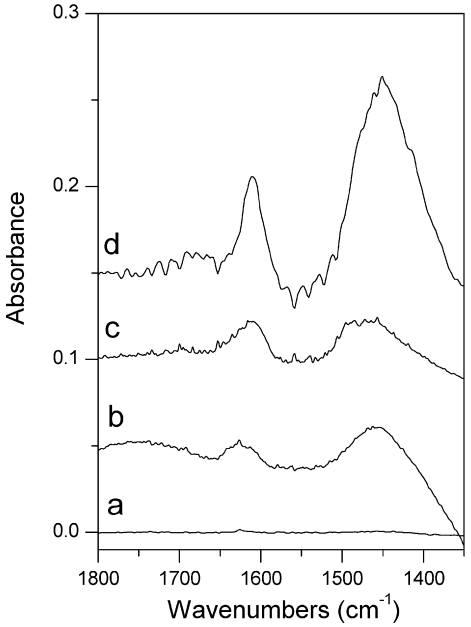

Fig. 10. Normalized FT-IR difference spectra recorded after dosing 0.4 mbar of NH_3 at r.t. on samples V10Si-i (curve a); V5Si (curve b); V10Si (curve c) and V28Si (curve d).

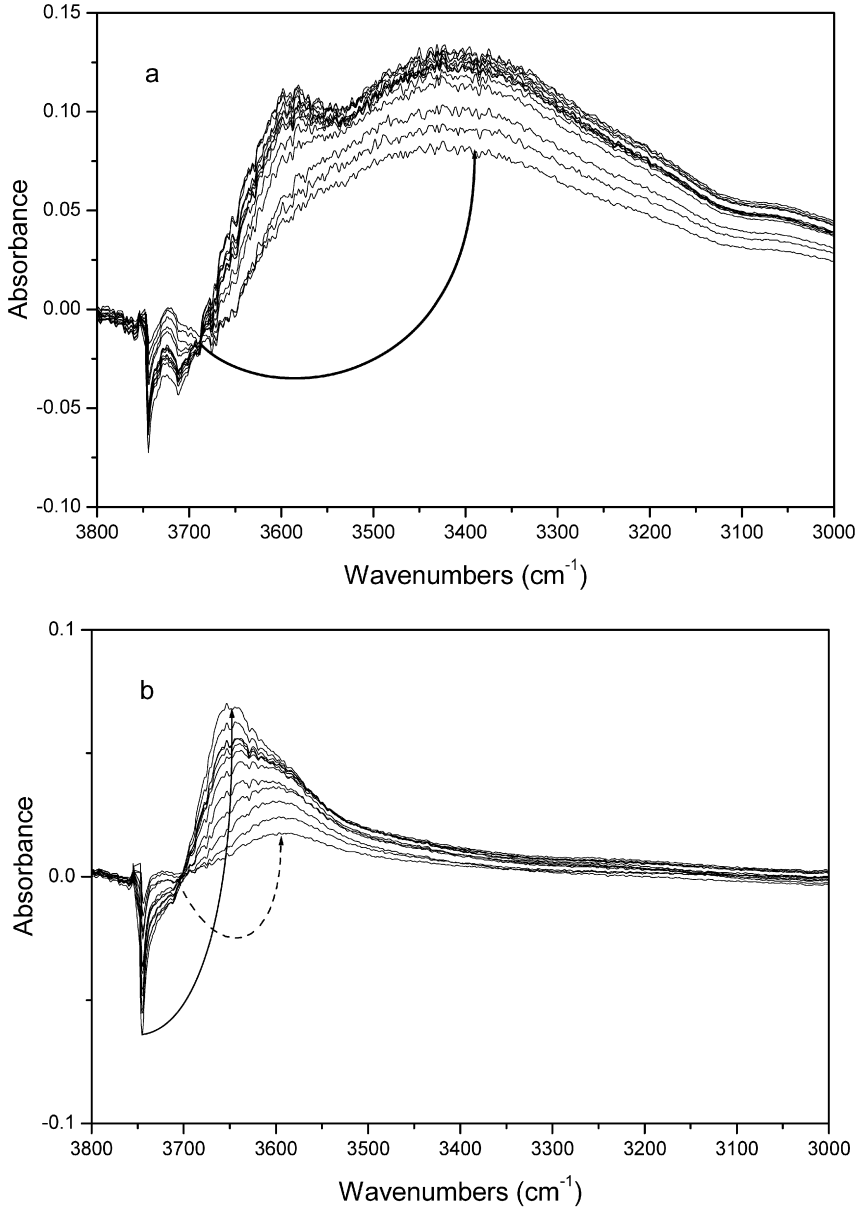

Fig. 11. FT-IR difference spectra recorded after dosing CO at the temperature of liquid N_2 on sample V10Si out gassed at 150 °C (section a) and 500 °C (section b). CO partial pressures in the 0.05–15.0 mbar range.

posed: isolated SiOH < H-bonded SiOH < V–OH. More acidic species, like V–OH, dehydroxylated first, leaving some Lewis sites accessible to ammonia (band at 1606 cm^{-1}) on the surface.

Fig. 10 shows the normalized difference spectra, recorded after dosing ca. 0.4 mbar ammonia on different samples outgassed at 500 °C. NH_3 did not adsorb on V-10Si-i (curve a), in agreement with its low surface area; at higher vanadium content (curves b to d), the bands of ammonia adsorbed on both Lewis acid and Brønsted acid sites increased in intensity, due to the presence of acidic sites at the catalyst surface.

To better evaluate the nature of surface hydroxyls, CO adsorption was studied at the temperature of liquid nitrogen. Fig. 11 shows the difference spectra in the hydroxyl range, obtained after subtracting that of the bare sample, on sample V10Si outgassed at 150 (a) and 500 °C (b). Dosing CO on sample V10Si out-gassed at 150 °C (a) resulted in the formation of a broad absorption band at below 3600 cm^{-1}, assigned to hydroxyls interacting with CO molecules through H bonding. The more acidic the hydroxyls, the greater the observed shift [53]; species absorbing at 3675 cm^{-1} shifted to 3415 cm^{-1} ($\Delta\nu = 3675–3415 = 260$ cm^{-1}), whereas the H-bonded silanol band at 3710 cm^{-1} shifted to 3590 cm^{-1} ($\Delta\nu = 120$ cm^{-1}), as on silica. When the sample was outgassed at 500 °C (b), only the features of free silanols (band at 3745 cm^{-1}, shifting to 3645 cm^{-1}, with $\Delta\nu = 100$ cm^{-1}) and of residual H-bonded silanols (band at 3710 cm^{-1}, shifting to 3590 cm^{-1}, with $\Delta\nu = 120$ cm^{-1}) remained, indicating the preferential elimination of more acidic hydroxyls (V–OH species originally absorbing at 3675 cm^{-1}).

The high concentration of Si–OH groups and also of V–OH, given the relatively low surface area of the samples, is likely due to the development of a metastable oxide at the high temperature at which oxide formation occurred in the flame. The adopted preparation method led to materials in which V was partly embedded in the silica matrix and the rapid dehydration forced the structure to adopt V–O–Si and Si–O–Si strained bonds, which were rapidly hydrolyzed during cooling in wet air. This gave rise to V–OH species with acidity close to that of the V–OH found in V/silicalite [49] and V supported on high surface SiO_2 [48], but formed through a different process. An alternative explanation can be sought in the complex radical reactions occurring in the flame, where OH can attack the V and Si precursors as well as peroxide radicals, which subsequently evolve into the oxide. The intermediate hydroxyl should decompose by dehydration, but this cannot occur if rapid quenching occurs. Similar phenomena have been observed with different materials with residual carbonate species, although the flame temperature during synthesis was far higher than that of carbonate decomposition [24–26]. This effect would explain the high concentration of hydroxyls in our FP samples and the stabilization of vanadium into the silica matrix.

3.7. Catalytic activity

The catalytic activity of all samples was compared both by co-feeding propane and oxygen (co-feeding mode) and under anaerobic conditions corresponding to the first step of the cyclic redox-decoupling mode, in which the feed of the hydrocarbon is alternated with that of oxygen. The latter procedure allows the investigator to alternate reaction and regeneration steps, thereby preventing the co-presence of propane and oxygen. This provides for safer operation and can improve catalyst selectivity to propylene.

3.7.1. Anaerobic conditions

Figs. 12a and 12b show the performance of the V10Si catalyst, at 550 °C, as a function of time on stream (TOS) during the first reduction half-cycle. The initial conversion was close to 14%, but declined rapidly with increasing TOS. Finally, the catalyst attained a steady state, with 6% conversion, due to the dehydrogenation of propane to propylene. Simultaneously, the formation of CO and CO_2 decreased, approaching values close to zero, while the selectivity to propylene increased correspondingly, from 78 to 90%. Remarkably, the selectivity to propylene or to CO_x was fully stable after 30 min TOS, although variations were very small. Therefore, after 30 min, the catalysts had not yet totally consumed the bulk oxygen available for the redox reactions. The concentration of H_2 was initially nil, but then increased, ultimately reaching a value close to 1.8 mol%.

These results indicate that at the beginning of the reducing cycle, the catalyst produced propylene through ODH, then shifted progressively to a dehydrogenation (DH) catalyst, becoming more and more reduced. But it is important to note that for very small TOS values, when there was no H_2 production and the catalyst acted as a stoichiometric oxidant, the selectivity to propylene was almost 80% for a propane conversion

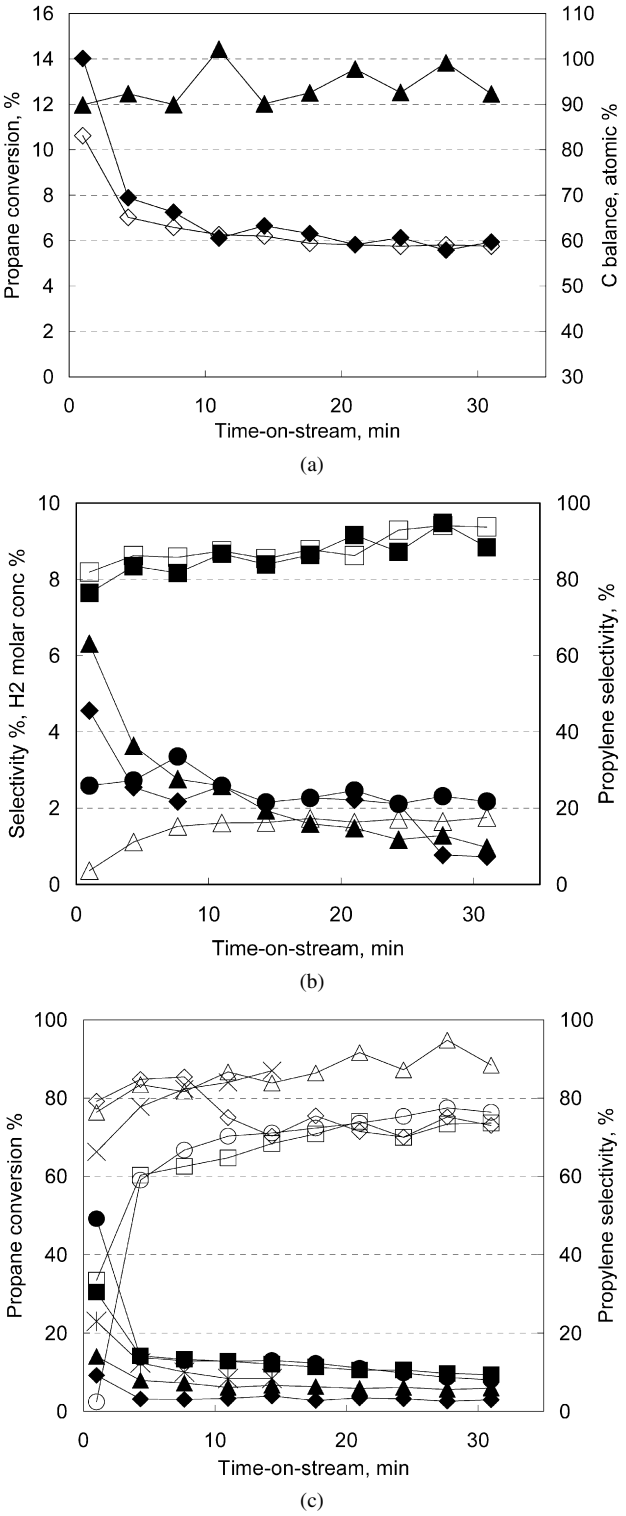

Fig. 12. Effect of time on-stream during the anaerobic reducing step (half-cycle) over catalyst V10Si on: (a) propane conversion (◆) and at% C balance (▲) during the first reducing half-cycle, and propane conversion during the second reducing half-cycle (◇) for catalyst V10Si; (b) molar selectivity to propylene (■), carbon monoxide (◆), carbon dioxide (▲), light hydrocarbons (●), out coming H_2 concentration (mol%) (△) and selectivity to propylene during the second reducing half-cycle (□). (c) Propane conversion (full symbols) and molar selectivity to propylene (open symbols), for catalysts V5Si (◆, ◇), V10Si (▲, △), V28Si (■, □) and V50Si (●, ○). $T = 550$ °C, gas contact time 2 s. Propane conversion (⋇) and molar selectivity to propylene (×) for catalyst V10Si at 550 °C and gas contact time 4 s.

of 12%. This confirms that the redox-decoupling concept may indeed lead to an effective improvement of selectivity with respect to the co-feeding operation (*vide infra*).

Figs. 12a and 12b also show the catalytic performance for the second reduction half-cycle, that is, after the reoxidation treatment in air at 550 °C after the first cycle. The activity was slightly lower than that observed after the first cycle. This effect can be attributed to incomplete reoxidation of the reduced vanadium species, to incomplete removal of coke, or again to some rearrangement of the V oxide structure as a consequence of the highly exothermal oxidation treatment and the high local temperature developing on the catalyst surface during this treatment.

Fig. 12c summarizes the catalytic performance for increasing amounts of vanadium oxide. The progressive reduction of catalyst led to improved selectivity to propylene, due to both lower consecutive propylene oxidation and an increased contribution of propane dehydrogenation. The higher the V content, the greater the propane conversion, both at the very beginning of the reduction step (i.e., fully oxidized catalyst) and after 30 min TOS. But the activity after 30 min was not directly proportional to the V content; in fact, the conversion achieved with the V50Si sample matched that achieved with the V28Si sample. This effect may be attributed to the significantly lower SSA value of the V50Si catalyst compared with the V28Si sample.

Furthermore, it is noteworthy that whereas V5Si and V10Si allowed stable performance already after 10 min TOS, V28Si and V50Si were not completely stable even after 30 min. This finding can be attributed to two contrasting factors: (i) the progressive migration of bulk O^{2-} toward the surface, which still allowed the catalyst to sustain the ODH reaction even after prolonged exposure to the hydrocarbon feed, and (ii) the progressive deactivation, most likely due to coke accumulation, resulting in a decline in catalyst activity.

For all of the catalysts, the amount of V oxide available for reduction was lower than the theoretical amount. Indeed, for V5Si, V10Si, and V28Si, the experimental weight loss (as calculated from the stoichiometry of reactions involved and from the integral values of propane conversion and selectivity to products) was approximately 25–30% that calculated for the complete reduction of V^{5+} to V^{3+}. This is likely due to the fact that a fraction of the V oxide was embedded inside the catalyst particles and thus not in contact with the gas phase. Only for the V50Si catalyst did the fraction of V oxide that delivered oxygen attain 70% of the theoretical value. Moreover, for V/Si/O catalysts prepared by the co-gelation procedure [30], <50% of V oxide was available for the reaction under anaerobic conditions. It should be noted that V^{4+} concentration, calculated semiquantitatively from EPR data, seemed to increase abruptly from V5Si to V10Si, then levelled off with further increases in V loading. This can be explained by considering that when V is highly dispersed and incorporated into the silica matrix, it can more readily assume different oxidation states. In contrast, when significant V_2O_5 segregation occurs, a similar concentration of V^{4+} is expected despite the increased V loading.

The hypothesis of coke accumulation on the catalyst during anaerobic operation is supported by various experimental evidence, including (i) the low final activity of V28Si and V50Si, in line with FT-IR data on NH_3 and CO adsorption (*vide supra*); (ii) the experimental trend for H_2 formation (*vide infra*); and (iii) the selectivity to propylene (close to 75%) after prolonged exposure to the hydrocarbon feed, which was lower than that (90–95%) obtained with V10Si (although comparable with that of V5Si). The lower selectivity to the olefin was due to the poorer C balance, on average 80–85% for V28Si and V50Si but close to 95% for V10Si (Fig. 12a). This indicates the accumulation of coke on the catalyst surface. It is noteworthy that also for V5Si, the average C balance at 20–30 min TOS was close to 85% and the selectivity to propylene was close to 75%. This indicates that under anaerobic conditions, the accumulation of coke was favored with those catalysts with the lowest (V5Si) and the highest (V28Si and V50Si) vanadium oxide content, demonstrating the relevant role of the support acidity in promoting coke formation with V5Si and also of the acidity of the V sites with high a degree of aggregation (i.e., in bulk vanadium oxide) with V28Si and V50Si.

Further evidence of the formation of coke under anaerobic conditions was provided by the Raman spectra of spent catalysts (i.e., analyzed after the reducing step). Typical Raman features associated with the presence of coke were observed (Fig. 13). Furthermore, during the half-cycle reoxidation step for the reduced catalyst, the formation of CO_2, along with minor amounts of CO, was observed. The formation of these compounds was greatest during the first 8–10 min of treatment and became practically nil after approximately 15 min.

Taking the initial performance into consideration, the high activity of V28Si and V50Si also corresponded to a lower selectivity to propylene. This is the consequence of the higher alkane conversion and greater degree of V aggregation, both of which favor the consecutive reaction of propylene combustion. The V5Si and V10Si catalysts demonstrated the greatest initial selectivity; however, the former sample showed a decline in selectivity after the initial period. Thus, V10Si seems to represent the best compromise between the need to expose as much as possible of the active component at the catalyst surface and the need to maintain a high degree of V oxide dispersion.

To compare the performance of the differently loaded materials (with strongly different activities) at a similar degree of conversion and a similar degree of reduction, we carried out tests with the V10Si catalyst at a gas contact time of 4 s (Fig. 12c). Under these conditions, the fully oxidized V10Si catalyst allowed 23% propane conversion, with 66% selectivity to propylene. This result can be compared with the performance of the fully oxidized V28Si catalyst, which allowed 30% propane conversion and 33% selectivity to propylene at 2 s of gas contact time. It is evident that the V10Si catalyst, which does not contain bulk vanadium oxide, was more selective to propylene than V28Si, which contains a certain amount of bulk vanadium oxide (as determined by spectroscopic analysis, such as Raman).

The observed H_2 formation (Fig. 14a) was close to zero for all catalysts at the beginning of the reaction and increased progressively thereafter. The amount of hydrogen produced was greater for the samples with higher V oxide content, in agree-

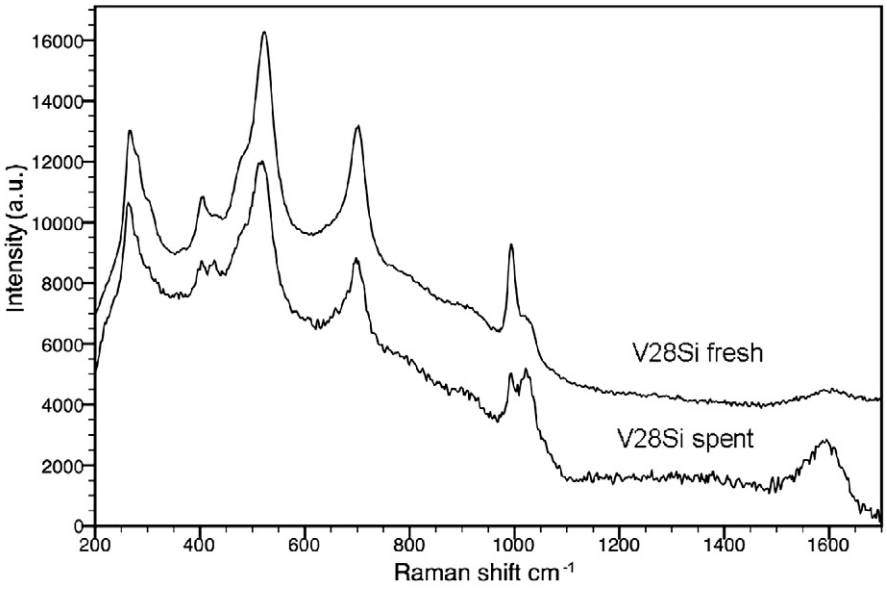

Fig. 13. Raman spectra of V28Si, fresh sample and after run under anaerobic conditions.

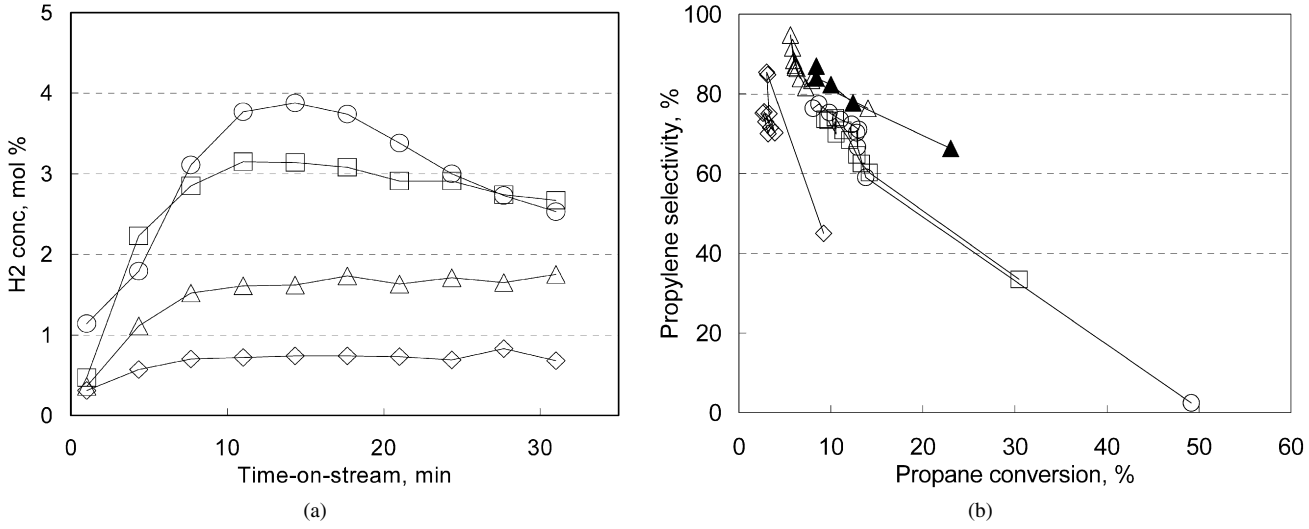

(a) (b)

Fig. 14. Effect of time on-stream on: (a) hydrogen concentration in the out coming stream and (b) propylene molar selectivity vs. conversion, during the anaerobic reducing step (half-cycle) for catalysts V5Si (◇), V10Si (△, gas contact time 2 s; ▲, gas contact time 4 s), V28Si (□) and V50Si (○). $T = 550\,^{\circ}C$, gas contact time 2 s.

ment with the higher activity in propane DH (Fig. 12c). However, although with V5Si and V10Si the formation of hydrogen remained constant after 10 min TOS, with V28Si and especially with V50Si, the formation of H_2 reached a maximum at ca. 15 min TOS. This was clearly due to coke accumulation. However, it is worth noting that in for V28Si and V50Si, the amount of H_2 produced was much greater than that corresponding to propylene formation (i.e., 2.7% vs. a theoretical 1.6 mol% for V28Si and 2.7% vs. a theoretical 1.4 mol% for V50Si) after 30 min TOS. The difference was much greater (especially with V50Si) when considering the maximum concentration of H_2 at 15 min TOS. This points to an additional contribution to H_2 formation besides propane DH. The relative importance of this further reaction increased with increasing V oxide loading. The additional contribution to H_2 evolution may come from coke formation, which, on the other hand, decreased the instantaneous propane conversion and thus the total amount of H_2 produced at higher TOS values.

Finally, Fig. 14b compares the selectivity and conversion for all of the catalysts under anaerobic conditions. Although the plot may be somewhat misleading (due to the fact that for a given level of conversion, the catalysts had been exposed to the reducing stream for different times, and thus they had different oxidation levels), nevertheless the results confirm the better selectivity to propylene achieved with V10Si. For the latter catalyst, the figure also reports the previously mentioned activity data at a gas contact time of 4 s.

3.7.2. Co-feed conditions

Figs. 15a and 15b summarize the performance of the V10Si sample under co-feed conditions. Total O_2 conversion was reached already at 450 °C, with a corresponding 26% propane

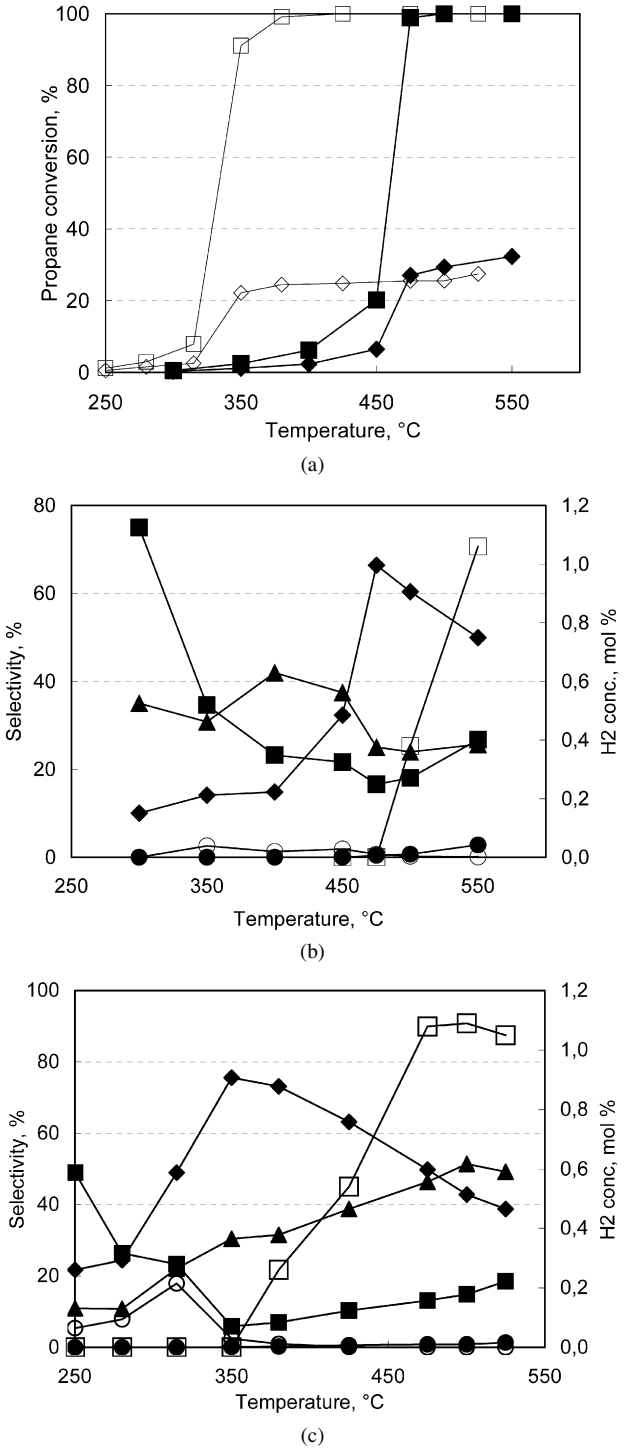

Fig. 15. Effect of reaction temperature: (a) on propane (◆) and oxygen (■) conversion in the co-feed mode over catalysts V10Si (full symbols), and V50Si (empty symbols); (b) on molar selectivity to propylene (■), carbon monoxide (◆), carbon dioxide (▲), light hydrocarbons (●), acetic acid (○) and to the outlet H_2 mol% concentration (□) in the co-feed mode over catalyst V10Si. (c) As for (b) but over catalyst V50Si.

conversion. An increase in temperature led to a further increase in propane conversion, mainly because of the additional contribution of propane dehydrogenation. Selectivity to propylene was good (75%) only for very low propane conversion (<1%), but decreased with increasing reaction temperature and

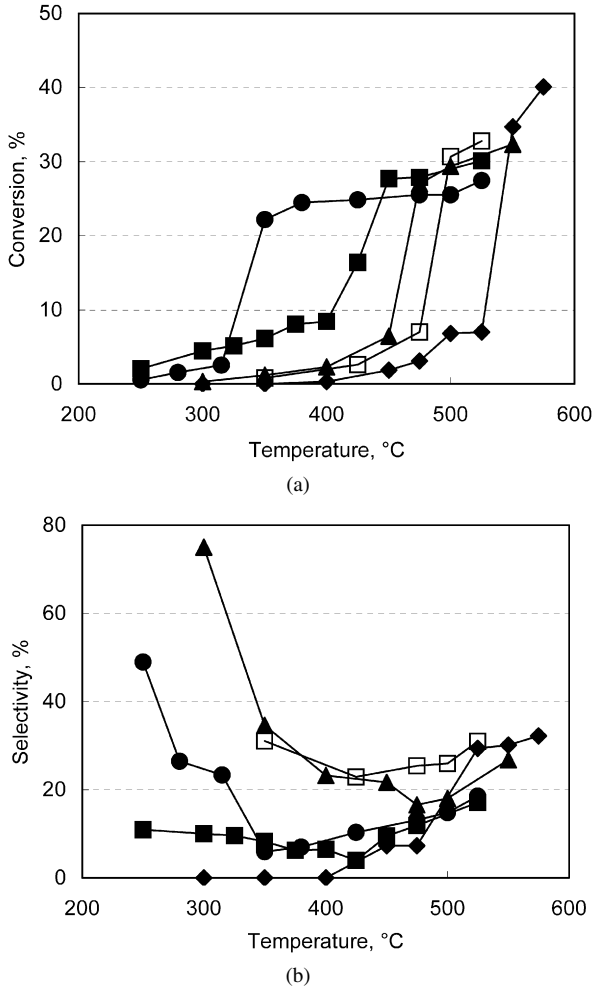

Fig. 16. Effect of reaction temperature (a) on propane conversion and (b) on molar selectivity to propylene. Co-feed mode, catalysts V5Si (◆), V10Si (▲), V28Si (■), V50Si (●) and V10Si-i (□).

propane conversion. Above 480 °C, however, the contribution of propane dehydrogenation (as evident from the formation of molecular hydrogen) led to better selectivity to propylene and to lower selectivity to CO and CO_2. This catalyst also demonstrated the best selectivity under co-feed conditions (*vide supra*).

Besides its greater activity due to the higher V-loading (*vide infra*), the main difference with V50Si concerns selectivity to CO and CO_2 at high temperature (Figs. 15a and 15c). It can be seen that, despite the fact that total O_2 conversion had already been reached at around 350 °C, a further temperature increase led to increased selectivity to CO_2 and decreased selectivity to CO. In a previous work [54], this was attributed to the activity of reduced bulk vanadium oxides, which catalyze the water-gas shift (WGS) reaction. Another difference concerns the significant selectivity to acetic acid. In the previous study [54], when the loading of V oxide over either silica or alumina was lower than or close to the theoretical monolayer, the catalysts exhibited no activity for the WGS reaction. The same effect was seen with the present catalysts.

Figs. 16a and 16b compare propane conversion and selectivity to propylene as a function of reaction temperature for all

catalysts (with tests run before the anaerobic tests). Activity was proportional to the V content. The best selectivity to propylene was obtained with the V10Si catalyst. The catalyst with the lowest V content (V5Si) was completely unselective to propylene at low conversion, forming CO_2 almost exclusively. Both V28Si and V50Si were less selective to propylene compared with V10Si. For all catalysts, in the low-temperature range selectivity decreased with increasing propane conversion, due to the contribution of the consecutive reaction of propylene combustion. An increase in selectivity was found once total oxygen conversion was attained, due to the increased contribution of propane dehydrogenation. The catalytic performance of these silica-based materials was obviously worse than that of other siliceous materials (MCF or MCM-41), in which V incorporation or grafting, aimed at obtaining very disperse (isolated) species, led to samples with surprisingly high selectivity and productivity to olefin [55]. The same authors pointed out that the latter samples demonstrated much better performance than catalysts prepared by conventional impregnation of vanadium oxide over silica.

3.7.3. Comparison between FP-prepared and impregnated catalysts

Fig. 17 compares the performance under anaerobic conditions of V10Si and of the reference catalyst V10Si-i, obtained by impregnation of the FP-prepared silica. The V oxide should be prevalently dispersed over the silica surface with V10Si-i, predominately in the form of bulk vanadia aggregates, as shown in the characterization section. In contrast, although the total amount of vanadium was the same in both samples, it should be embedded in the bulk, at least in part, with the V10Si sample. The two samples showed very comparable initial activity, notwithstanding the remarkably higher SSA value of the FP-prepared sample with respect to that of V10Si-i. This is likely due to the fact that more V oxide was available with the V10Si-i catalyst (being deposited over silica) than with the FP-prepared catalyst. In fact, with the V10Si-i catalyst, the weight loss (calculated from the stoichiometry of the reactions occurring under anaerobic conditions) corresponded to approximately 50% of the theoretical value (calculated by assuming a complete reduction of V_2O_5 into V_2O_3) and was almost twice that found for the V10Si catalyst.

Propane conversion followed the same trend for the two catalysts (Fig. 17a), but the selectivity was clearly better with the FP-prepared catalyst than with the impregnated catalyst (Fig. 17b). The difference in selectivity was evident at the beginning of the reduction period, when the catalyst was still fully oxidized, and then diminished as long as the catalyst was reduced progressively. The difference at the beginning of the reduction period confirms the different nature of the V species responsible of the ODH of propane.

Fig. 17 also shows the behavior of catalyst V28Si. This sample demonstrated the presence of crystalline V_2O_5 as well as an overall amount of vanadium oxide available for reaction (as measured from the comparison between the theoretical weight loss and the experimental one in anaerobic tests) of ca. 8 wt%, not far from the 5 wt% of the V10Si-i catalyst. V28Si was not only more active, but also clearly more selective than V10Si-i. This provides further evidence of the overall better performance of the catalysts prepared by the FP method.

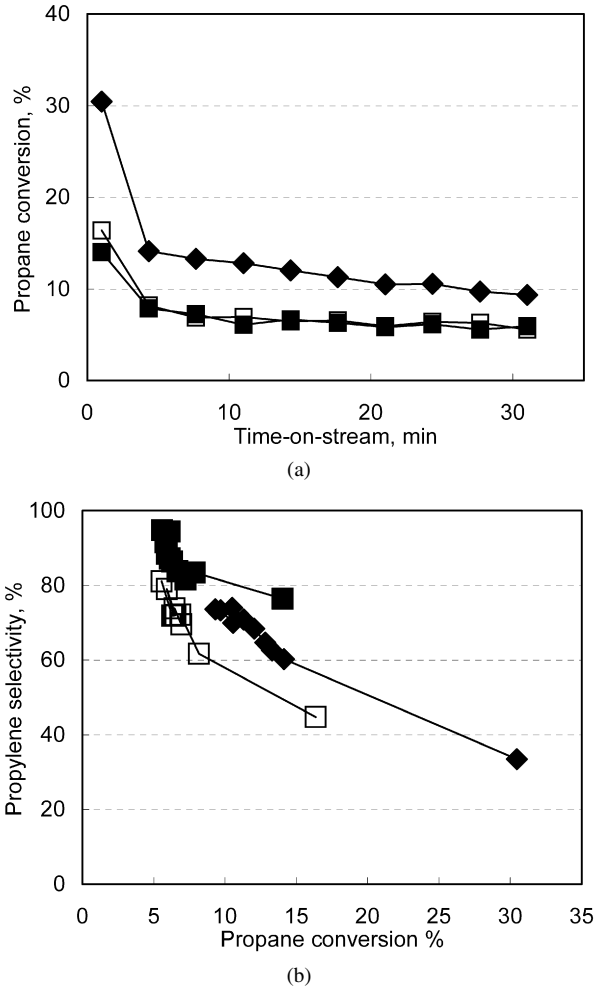

Fig. 17. (a) Effect of time on-stream during the anaerobic reducing step (half-cycle) on propane conversion. (b) Molar selectivity to propylene vs. propane conversion, for V10Si (■), V10Si-i (□) and V28Si (◆) catalysts at $T = 550\,^{\circ}C$.

3.7.4. Comparison between anaerobic and co-feed reaction conditions

Fig. 18 compares the selectivity to propylene versus propane conversion under co-feed and anaerobic conditions. It is noteworthy that in the former case, the conversion varied with changes in temperature, whereas under reducing conditions, it changed progressively during the permanence at isothermal conditions ($T = 550\,^{\circ}C$) in the reducing stream. Therefore, the most significant comparison was that of the still-oxidized catalysts, that is, at the very beginning of the reducing time. For each catalyst, this corresponds to the greatest instantaneous conversion of propane. The comparison clearly demonstrates that operation under anaerobic conditions may provide advantages in terms of selectivity with respect to the co-feed operation. Specifically, whereas for V28Si and V50Si, the selectivity to propylene achieved in the presence and absence of oxygen (in the latter case, for the fully oxidized catalyst) did not dif-

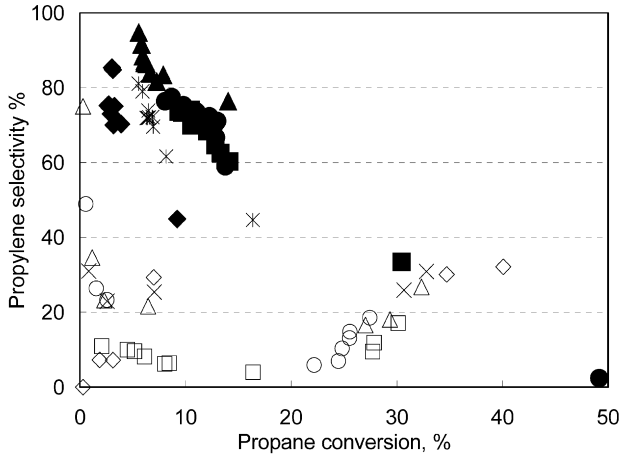

Fig. 18. Molar selectivity to propylene vs. propane conversion for the anaerobic (full symbols) and co-feed (open symbols) modes. Catalysts V5Si (◆, ◇), V10Si (▲, △), V28Si (■, □), V50Si (●, ○) and V10Si-i (⋇, ×). $T = 550\,^{\circ}C$, gas contact time 2 s.

fer much, for V5Si and V10Si, significantly greater selectivity was obtained under anaerobic conditions. Especially with the latter catalyst, selectivity to propylene at the beginning of the reduction time (at ca. 15% conversion) was >60% greater than that obtained in the presence of oxygen at comparable propane conversion. In fact, Figs. 15a and 15b show that between 450 and 475 °C in the co-feed mode, propane conversion increased from 7 to 27%, oxygen conversion increased from 20 to 98%, and selectivity to propylene decreased from 22 to 17%. The latter value was considerably lower than that obtained with the V10Si sample in the absence of molecular oxygen.

In a previous work on V_2O_5–SiO_2 catalysts with VO_x dispersed in the gel [30], the reaction under anaerobic conditions led to improved selectivity to propylene (around 25–30% higher for a 35–40% propane conversion) compared with that under co-feed conditions. The best selectivity was achieved at the very beginning of the reduction step, when the catalyst was still fully oxidized and acted as a true ODH catalyst even in the absence of molecular oxygen. Remarkably, this property was specific to the V_2O_5–SiO_2 system. In fact, when vanadium oxide was supported over either alumina or titania, no effective improvement in propylene selectivity was observed for the anaerobic operation with respect to the co-feed mode [17].

In the present investigation, the best performance in propane ODH under both co-feed and anaerobic conditions was observed with the catalyst containing 10 wt% V_2O_5. Only VO_x isolated species (with no vanadium-oxide aggregates) were present in this catalyst, as determined by Raman spectroscopy (*vide supra*). This is an advantage associated with the FP preparation technique, which allows higher V loading before V_2O_5 begins to segregate. In contrast, when silica is used as a support, the amount of vanadium oxide exceeds that required for monolayer formation, leading to V_2O_5 formation at V loadings below those for the present FP-prepared samples. This is likely due to the peculiarity of the latter samples, which exhibited much higher-than-expected surface Si–OH concentrations that decreased with increasing V loadings, as shown by FT-IR data (*vide supra*). Furthermore, as evidenced by the spectroscopic characterization, the development of V–O–Si bonds confirms that a prerequisite for the formation of isolated VO_x species was the presence of a high concentration of surface hydroxyl groups. It can be hypothesized that after the high-temperature flash vaporization and pyrolysis of the precursor organic solution in the flame, the development of a metastable oxide was followed by the opening of strained Me–O–Me bonds and generation of Me–OH moieties during quenching in the wet atmosphere. On the other hand, the FP method favored the formation of V–O–Si bonds and thus the generation of isolated VO_x species at concentrations greater than are usually obtained with impregnated silica. The successive calcination treatment at 550 °C also may have favored the development of additional V–O–Si bonds and the generation of isolated VO_x species. This also occurred with the V5Si catalyst, in which, however, a greater fraction of exposed silica caused a deterioration of performance and resulting lower selectivity to propylene, due to a more abundant formation of carbon oxides under the co-feed mode and of coke under anaerobic conditions. In contrast, with the V28Si and V50Si samples, the characterization clearly showed the formation of bulk vanadia aggregates, which were responsible for the formation of carbon oxides and acetic acid in the co-feed mode and of carbon oxides under anaerobic reaction conditions.

Comparing the catalyst prepared with the sol–gel method containing 7 wt% V_2O_5 [30] and the V10Si catalyst reported here demonstrates that the two samples behaved similarly under anaerobic conditions (with very similar plots of selectivity to propylene as a function of conversion), but the sol–gel catalyst gave better selectivity than the FP catalyst under co-feed conditions. This difference can be attributed to the greater exposure of the V–OH and Si–OH groups for the FP-prepared catalyst. But under anaerobic conditions, the V10Si catalyst demonstrated much greater selectivity to propylene than the corresponding sol–gel catalyst. This indicates that the hydroxyl groups did not play a negative role in selectivity when the reaction was carried out in the absence of molecular oxygen.

Our findings confirm significant differences in the nature of V sites of the FP-prepared samples and the impregnated samples and those in samples prepared by conventional techniques, such as sol–gel [30]. Indeed, high V dispersion was evident for the FP-prepared samples, at least up to 10 wt% V_2O_5. In the V10Si catalyst, no segregated vanadia was detected by XRD, Raman, or FT-IR analysis, and no V^{4+} ferromagnetic domains were demonstrated on EPR spectroscopy, in contrast to the V10Si-i sample (Fig. 4). These EPR results provide insight into the local structure of the V-based active sites. Indeed, the EPR features due to V^{4+} maintained a constant profile but grew markedly in intensity after reaction under anaerobic conditions (Fig. 3), indicating not only that a considerable amount of V^{4+}–based species formed on reduction of V^{5+} during the catalytic process without reoxidation, but also that in these species, the V^{4+}–O bond was slightly stronger in V10Si than in V10Si-i (*vide supra*). This finding suggests that the bonds between surface V and O likely were stronger in the former sample than in the latter sample also in the V^{5+} active cen-

ters. This is in agreement with the activity data showing that the samples with stronger V^{4+} to O bonds were characterized by lower oxygen availability (i.e., lower activity) but higher selectivity.

Comparing the V10Si and V10Si-i catalysts also provided additional insights. The two samples exhibited very similar performance in the co-feed mode, but the V10Si sample demonstrated higher selectivity to propylene under anaerobic conditions. Because the two catalysts exhibited very similar activity, this difference can be attributed to the different nature of the VO_x species. Of note, IR bands due to vibration of SiO_4 groups perturbed by the presence of neighboring V ions were not seen for the V10Si-i sample. This indicates that only the FP method (involving concomitant FP of the V–Si complex species) led to the partial incorporation of V ions in silica. The hydrolysis of surface Me–O–Me strained bonds can lead to the exposure of subsurface VO_x species. These species are located in a nest surrounded by Si–OH species, which also contribute to the isolation of the V ion. The finding of a greater concentration of isolated VO_x species in V10Si with respect to V10Si-i demonstrates the positive effect on selectivity to propylene, but only when the reaction was carried out under anaerobic conditions. The same effect was observed for V_2O_5/SiO_2 co-gel systems [30] and was attributed to the fact that when the reaction is carried out in the presence of molecular oxygen, the generation of unselective O^{2-} species (rather than the dispersion of the active sites) controls the selectivity of the process. When instead the reaction is carried out in the absence of molecular oxygen, the better isolation of the active sites may effectively control the availability of surface O^{2-} sites and thereby limit the consecutive and parallel total combustion reactions.

Fig. 18 shows that the V10Si-i catalyst gave better selectivity to propylene under anaerobic conditions than in the co-feed mode. The gain in selectivity was around 25–30% at 15–20% propane conversion. This figure also shows a considerably greater improvement in selectivity (by ca. 50–60%) with the V10Si catalyst. It is evident that the concomitant generation of the V and Si oxides achieved by the FP method led to a system that provides superior performance under anaerobic conditions due to the increased concentration of isolated VO_x sites.

4. Conclusion

VO_x/SiO_2 catalysts with different V loading were prepared by the FP technique. Their physicochemical and catalytic properties for the ODH of propane differed significantly from those of a comparative sample prepared by impregnation. Much higher V dispersion was achieved for the FP-prepared sample compared with the impregnated catalyst at the same V loading. Higher selectivity to propylene also was achieved with the FP samples, especially under anaerobic conditions. The active sites of the FP-prepared catalysts contained highly dispersed $V^{5+}O$ groups, partly incorporated into the silica matrix and poorly interacting with one another. EPR characterization allowed identification of the V^{4+} site structure as consisting of $V^{4+}O$ groups in the center of a surface array of oxygen atoms. High V site isolation was found, especially for the FP samples at up to 10 wt% V loading, along with the absence of oligomeric species. But at higher V loadings, bulk vanadia began to segregate, with a consequent decrease in catalyst selectivity. The unexpectedly high surface hydroxyl concentrations detected on the FP samples despite the high calcination temperature attained during synthesis, very likely helps stabilize these dispersed V species. Thus, the advantage of the present FP preparation method over other preparation procedures is the possibility of hosting higher V concentrations without V_2O_5 segregation, thereby permitting greater selectivity compared with that provided by traditionally prepared catalysts.

Acknowledgments

This work was supported by the Italian Ministry of University and Research through the COFIN program (2005038244). The authors thank INSTM for a PhD grant to A.C., the Norwegian Research Council for a PhD grant and travel grant for H.D. through the KOSK program, and S. Cappelli for EPR spectra collection.

References

[1] F. Cavani, F. Trifirò, Catal. Today 24 (1995) 307.
[2] E.A. Mamedov, V. Cortes-Corberan, Appl. Catal. A 127 (1995) 1.
[3] T. Blasco, J.M. Lopez Nieto, Appl. Catal. A 157 (1997) 117.
[4] F. Cavani, F. Trifirò, in: M. Baerns (Ed.), Basic Principles in Applied Catalysis, in: Ser. Chem. Phys., vol. 75, Springer, Berlin, 2003, p. 21.
[5] N. Ballarini, F. Cavani, A. Cericola, Catal. Today 127 (2007) 113.
[6] A. Bottino, G. Capannelli, A. Comite, S. Storace, R. Di Felice, Chem. Eng. J. 94 (2003) 11.
[7] M.D. Argyle, K. Chen, A.T. Bell, E. Iglesia, J. Catal. 208 (2002) 139.
[8] T. Blasco, A. Galli, J.M. Lòpez Nieto, F. Trifirò, J. Catal. 169 (1997) 203.
[9] Z. Zhao, Y. Yamada, A. Ueda, H. Sakurai, T. Kobayashi, Catal. Today 93–95 (2004) 163.
[10] M.V. Martìnez-Huerta, X. Gao, H. Tian, I.E. Wachs, J.L.G. Fierro, M.A. Bañares, Catal. Today 118 (2006) 279.
[11] E.V. Kondratenko, N. Steinfeldt, M. Baerns, Phys. Chem. Chem. Phys. 8 (2006) 1624.
[12] D. Shee, T.V. Malleswara Rao, G. Deo, Catal. Today 118 (2006) 288.
[13] H. Tian, E.I. Ross, I.E. Wachs, J. Phys. Chem. B 110 (19) (2006) 9593.
[14] K. Chen, E. Iglesia, A.T. Bell, J. Catal. 192 (2000) 197.
[15] S. Dzwigaj, I. Gressel, B. Grzybowska, K. Samson, Catal. Today 114 (2006) 237.
[16] N. Ballarini, A. Battisti, F. Cavani, A. Cericola, C. Lucarelli, S. Racioppi, P. Arpentinier, Catal. Today 116 (2006) 313.
[17] N. Ballarini, F. Cavani, A. Cericola, C. Cortelli, M. Ferrari, F. Trifirò, G. Capannelli, A. Comite, R. Catani, U. Cornaro, Catal. Today 91–92 (2004) 99.
[18] M.D. Argyle, K. Chen, C. Resini, C. Krebs, A.T. Bell, E. Iglesia, J. Phys. Chem. B 108 (2004) 2345.
[19] N. Steinfeldt, D. Müller, H. Berndt, Appl. Catal. A Gen. 272 (2004) 201.
[20] X. Gao, S.R. Bare, J.L.G. Fierro, I.E. Wachs, J. Phys. Chem. B 103 (1999) 618.
[21] X. Gao, J.L.G. Fierro, I.E. Wachs, Langmuir 15 (1999) 3169.
[22] W.J. Stark, L. Mädler, S.E. Pratsinis, EP 1,378,489 A1 (2004), to ETH, Zurich.
[23] G.L. Chiarello, I. Rossetti, L. Forni, J. Catal. 236 (2005) 251.
[24] G.L. Chiarello, I. Rossetti, P. Lopinto, G. Migliavacca, L. Forni, Catal. Today 117 (2006) 549.
[25] G.L. Chiarello, I. Rossetti, L. Forni, P. Lopinto, G. Migliavacca, Appl. Catal. B Environ. 72 (2007) 218.

[26] G.L. Chiarello, I. Rossetti, L. Forni, P. Lopinto, G. Migliavacca, Appl. Catal. B Environ. 72 (2007) 227.
[27] R. Strobel, W.J. Stark, L. Mädler, S.E. Pratsinis, A. Baiker, J. Catal. 213 (2003) 296.
[28] L. Mädler, S.E. Pratsinis, J. Am. Ceram. Soc. 85 (7) (2002) 1713.
[29] R. Strobel, S.E. Pratsinis, A. Baiker, J. Mater. Chem. 15 (2005) 605.
[30] N. Ballarini, F. Cavani, M. Ferrari, R. Catani, U. Cornaro, J. Catal. 213 (2003) 95.
[31] R. Grabowski, S. Pietrzyk, J. Słoczynski, F. Genser, K. Wcisło, B. Grzybowska-Swierkosz, Appl. Catal. A 232 (2002) 277.
[32] G.E. Vrieland, C.B. Murchison, Appl. Catal. A 134 (1996) 101.
[33] D. Creaser, B. Andersson, R.R. Hudgins, P.L. Silveston, Chem. Eng. Sci. 54 (1999) 4365.
[34] D. Creaser, B. Andersson, R.R. Hudgins, P.L. Silveston, J. Catal. 182 (1999) 264.
[35] R.A.M. Giacomuzzi, M. Portinari, I. Rossetti, L. Forni, in: A. Corma, F.V. Melo, S. Mendioroz, J.L.G. Fierro (Eds.), Studies Surface Science and Catalysis, vol. 130, Elsevier, Amsterdam, 2000, p. 197.
[36] Advanced Selected Powder Diffraction Data, Miner. DBM (1–40), JCPDS, Swarthmore, PA, 1974–1992.
[37] W.J. Stark, L. Mädler, M. Maciejewski, S.E. Pratsinis, A. Baiker, Chem. Commun. (2003) 588.
[38] V.K. Sharma, A. Wokaun, A. Baiker, J. Phys. Chem. 90 (1986) 2715.
[39] A. Gervasini, G. Fornasari, G. Bellussi, Appl. Catal. A Gen. 83 (1992) 235.
[40] E.G. Derouane, A.J. Simoens, J.C. Védrine, Chem. Phys. Lett. 52 (1977) 549.
[41] E.G. Derouane, A. Simoens, C. Colin, G.A. Martin, J.A. Dalmon, J.C. Védrine, J. Catal. 52 (1978) 50.
[42] P.A. Jacobs, H. Nijs, J. Verdonck, E.G. Derouane, J.-P. Gilson, A.J. Simoens, J. Chem. Soc. Faraday Trans. I 75 (1979) 1196.
[43] C. Kittel, Introduction to Solid State Physics, third ed., Wiley, New York, 1967, p. 523.
[44] L. Bonneviot, D. Olivier, Ferromagnetic Resonance, in: B. Imelik, J.C. Védrine (Eds.), Catalyst Characterization. Physical Techniques for Solid Materials, Plenum Press, New York, 1994.
[45] T. Ono, H. Numata, J. Mol. Catal. A Chem. 116 (1997) 421.
[46] A. Khodakov, B. Olthof, A.T. Bell, E. Iglesia, J. Catal. 181 (1999) 205, and references therein.
[47] A. Klisińska, S. Loridant, B. Grzybowska, J. Stoch, I. Gressel, Appl. Catal. A Gen. 309 (2006) 17.
[48] D.E. Keller, T. Visser, F. Soulimani, D.C. Koninsberger, B.M. Weckhuysen, Vib. Spectrosc. 43 (2007) 140.
[49] S. Dzwigaj, P. Massiani, A. Davidson, M. Che, J. Mol. Catal. A Chem. 155 (2000) 169.
[50] A. Burneau, J.P. Gallas, in: A.P. Legrand (Ed.), The Surface Properties of Silica, 1999, p. 194, and references therein.
[51] B.A. Morrow, A.J. McFarlan, J. Phys. Chem. 96 (1992) 1395.
[52] J.A. Lercher, C. Gründling, G. Eder-Mirth, Catal. Today 27 (1996) 353.
[53] A. Zecchina, C. Otero Areán, Chem. Soc. Rev. 25 (1996) 187.
[54] N. Ballarini, A. Battisti, F. Cavani, A. Cericola, C. Cortelli, M. Ferrari, F. Trifirò, P. Arpentinier, Appl. Catal. A Gen. 307 (2006) 148.
[55] Y.-M. Liu, W.-L. Feng, T.-C. Li, H.-Y. He, W.-L. Dai, W. Huang, Y. Cao, K.-N. Fan, J. Catal. 239 (2006) 125.